Defective p53 engagement after the induction of DNA damage in cells deficient in topoisomerase 3β

Subhasis Mohanty*, Terrence Town[†‡], Tomohito Yagi*[§], Christina Scheidig*, Kelvin Y. Kwan[¶], Heather G. Allore[‖], Richard A. Flavell[†], and Albert C. Shaw*[,]**

*Section of Infectious Diseases, Departments of [‖]Internal Medicine and [†]Immunobiology, Yale University School of Medicine, New Haven, CT 06520; and [¶]Department of Neurobiology, Harvard Medical School, Boston, MA 02115

Communicated by Philip Leder, Harvard Medical School, Boston, MA, February 8, 2008 (received for review April 9, 2007)

The type IA topoisomerases have been implicated in the repair of dsDNA breaks by homologous recombination and in the resolution of stalled or damaged DNA replication forks; thus, these proteins play important roles in the maintenance of genomic stability. We studied the functions of one of the two mammalian type IA enzymes, Top3β, using murine embryonic fibroblasts (MEFs) derived from *top3*$\beta^{-/-}$ embryos. *top3*$\beta^{-/-}$ MEFs proliferated more slowly than *TOP3*$\beta^{+/+}$ control MEFs, demonstrated increased sensitivity to DNA-damaging agents such as ionizing and UV radiation, and had increased DNA double-strand breaks as manifested by increased γ-H2-AX phosphorylation. However, incomplete enforcement of the G_1–S cell cycle checkpoint was observed in *top3*$\beta^{-/-}$ MEFs. Notably, ataxia-telangiectasia, mutated (ATM)/ATM and Rad3-related (ATR)-dependent substrate phosphorylation after UV-B and ionizing radiation was impaired in *top3*$\beta^{-/-}$ versus *TOP3*$\beta^{+/+}$ control MEFs, and impaired up-regulation of total and Ser-18-phosphorylated p53 was observed in *top3*$\beta^{-/-}$ cells. Taken together, these results suggest an unanticipated role for Top3β beyond DNA repair in the activation of cellular responses to DNA damage.

cell cycle checkpoint | DNA repair | radiation sensitivity

The type I and type II DNA topoisomerases catalyze the sequential breakage and rejoining of single DNA strands or double helices, respectively, and play crucial functions in the maintenance of genomic stability (1). Type I enzymes break and rejoin DNA strands one at a time, whereas type II enzymes break and rejoin DNA strands two at a time in an ATP-dependent manner (2). In particular, the type IA topoisomerases, characterized by an active site tyrosyl residue linked to a DNA 5′ phosphoryl group (3), have emerged as potential key players in this role. Strains of the budding yeast *Saccharomyces cerevisiae* carrying a null mutation in the type IA topoismerase gene *TOP3* are slow growing, hyperrecombinogenic, and sensitive to DNA-damaging agents (4–7). In addition, null mutations in the *Schizosaccharomyces pombe TOP3* gene result in lethality caused by defects in chromosome segregation and DNA double-strand break repair (8–11).

Significantly, a DNA helicase of the RecQ family, Sgs1, was identified as a suppressor of *top3* nulls, and physical association of Top3 and Sgs1 has been observed (6, 12–14). Other than *SGS1*, mutations in a number of genes known to be involved in homologous recombination have also been shown to suppress the *top3* phenotype (15). These findings provide strong support for a model in which the type IA DNA topoisomerase mediates the resolution of intermediates of recombination/repair (6). Studies in the bacterium *Escherichia coli* are consistent with this interpretation (16, 17).

Notably, Top3 and Sgs1 are required for the resolution of double-Holliday junctions in the suppression of mitotic cross-over (18). Consistent with this hypothesis, the mammalian RecQ family helicase BLM forms a complex with one of the two type IA topoisomerases in mammals, Top3α, and is able to resolve a double-Holliday junction while suppressing cross-over events (19–23). Nonetheless, the functions of Top3α and the other mammalian Top3 ortholog, Top3β, remain incompletely understood. In this context, some insight has been obtained from studies using gene targeting in mice. Germ-line deletion of Top3α resulted in early embryonic lethality, whereas mice lacking Top3β function have shortened lifespan and a complex phenotype including shortened lifespan, aneuploidy in germ and somatic cells, age-associated lymphoproliferation, and evidence of autoimmunity (24–27). We have evaluated the growth, response to DNA-damaging agents, and cell cycle checkpoint control in cells deficient in Top3β.

Results

To elucidate the cellular functions of Top3β, we studied *TOP3*$\beta^{+/+}$ control and *top3*$\beta^{-/-}$ murine embryonic fibroblasts (MEFs) and observed that multiple independent lines of *top3*$\beta^{-/-}$ MEFs divided more slowly *in vitro* than *TOP3*$\beta^{+/+}$ control MEFs (Fig. 1*A*). To assess whether increased levels of DNA damage could contribute to the decreased growth rate of *top3*$\beta^{-/-}$ MEFs, we assessed the response of *top3*$\beta^{-/-}$ cells to DNA-damaging agents. *top3*$\beta^{-/-}$ MEFs displayed increased sensitivity to ionizing radiation relative to *TOP3*$\beta^{+/+}$ control MEFs and were also sensitive to UV-B radiation and hydroxyurea treatment (Fig. 1 *B–D*). Thus, Top3β deficiency results in increased genotoxin sensitivity.

To further evaluate levels of DNA damage in the context of Top3β deficiency, we used a fluorescent antibody reactive against phosphorylated γ-H2AX, which rapidly localizes to sites of DNA double-stranded breaks after the induction of DNA damage. Notably, in both flow cytometry and Western blot-based analysis, *top3*$\beta^{-/-}$ cells had increased levels of phosphorylated γ-H2AX relative to *TOP3*$\beta^{+/+}$ control MEFs after ionizing radiation treatment, with increased levels of γ-H2AX phosphorylation in *top3*$\beta^{-/-}$ cells also observed in the presence of the phosphatase inhibitor Calyculin A (Fig. 2). Taken together, these findings indicate that increased levels of DNA damage contributes to the delayed cell cycle progression observed in *top3*$\beta^{-/-}$ cells, consistent with a role for Top3β in the repair of DNA damage.

Alterations in cell cycle checkpoints may also contribute to increased sensitivity to DNA-damaging agents. Accordingly, we tested whether Top3β was required for the enforcement of such checkpoints. After irradiation, *top3*$\beta^{-/-}$ and *TOP3*$\beta^{+/+}$ control cells were either pulsed with BrdU 18 h later or stained with a fluorescent antibody recognizing phosphorylated histone H3 at

Author contributions: S.M., T.T., T.Y., C.S., R.A.F., and A.C.S. designed research; S.M., T.T., T.Y., C.S., and A.C.S. performed research; T.T., K.Y.K., and R.A.F. contributed new reagents/analytic tools; S.M., T.T., T.Y., C.S., H.G.A., and A.C.S. analyzed data; and S.M., T.T., H.G.A., and A.C.S. wrote the paper.

The authors declare no conflict of interest.

[‡]Present address: Departments of Neurosurgery and Biomedical Sciences, Maxine Dunitz Neurosurgical Institute, Cedars-Sinai Medical Center, Los Angeles, CA 90048.

[§]Present address: Division of Genomic Medical Sciences, Department of Molecular Medical Sciences, Kyoto Prefectural University of Medicine, Kyoto 602-8566, Japan.

**To whom correspondence should be addressed. E-mail: albert.shaw@yale.edu.

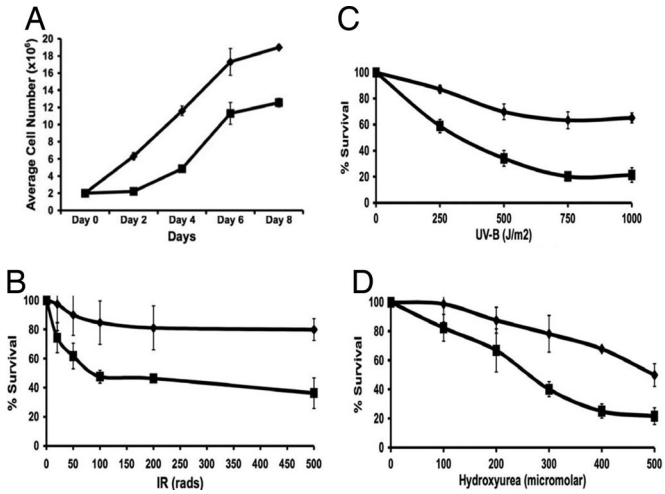

Fig. 1. Decreased growth and increased genotoxin sensitivity of *top3β*$^{-/-}$ MEFs. (*A*) Growth curves of *top3β*$^{-/-}$ (black squares) and *TOP3β*$^{+/+}$ control (WT) (black diamonds) MEFs; representative result of two independent experiments. Each data point represents the mean of duplicate samples, with standard error of the mean indicated by error bars. (*B–D*) Increased sensitivity of *top3β*$^{-/-}$ MEFs to ionizing radiation from a ^{137}Cs source (*B*), UV-B radiation (*C*), and HU (*D*) are depicted. Each data point represents the mean of triplicate samples, with standard error of the mean indicated. Results are representative of at least two experiments using independently derived *TOP3β*$^{+/+}$ control and *top3β*$^{-/-}$ MEFs.

various times, thereby assessing the integrity of the G_1/S and G_2/M checkpoints, respectively. Notably, whereas a slight increase in cells in G_1 was observed after treatment with ionizing radiation, we observed incomplete suppression of entry into S phase in *top3β*$^{-/-}$ cells, consistent with an incomplete defect in the G_1/S cell cycle checkpoint (Fig. 3*A*). In contrast, the G_2/M checkpoint appeared unperturbed in mutant cells, and we observed no clear difference either in the enforcement of this checkpoint or in recovery and reentry into mitosis 16 h after the induction of DNA damage (Fig. 3*D*). We also carried out BrdU pulse labeling studies on MEFs 1–2 h after UV-B irradiation, and in addition assessed radio-resistant DNA synthesis 1 h after ionizing radiation to determine whether S-phase DNA synthesis is appropriately suppressed after DNA damage. Notably, S-phase DNA synthesis appeared comparably suppressed in *top3β*$^{-/-}$ and *TOP3β*$^{+/+}$ control MEFs (Fig. 3 *B* and *C*). Thus, Top3β deficiency results in incomplete enforcement of the G_1/S checkpoint after DNA damage from ionizing radiation, suggesting a role for Top3β in mediating cell cycle control in addition to its role in the repair of DNA damage.

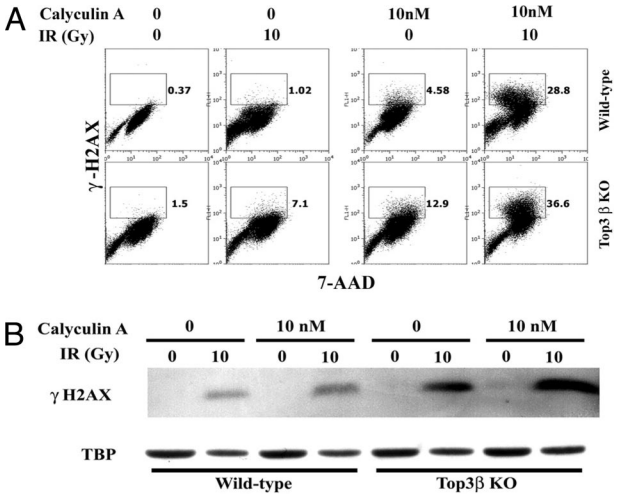

Fig. 2. Increased γ-H2AX phosphorylation in *top3β*$^{-/-}$ cells. Shown are flow cytometry profiles (*A*) and Western analyses (*B*) of acid-extracted nuclear proteins from *top3β*$^{-/-}$ and *TOP3β*$^{+/+}$ control (WT) MEFs before and 30 min after irradiation with 10 Gy from a ^{137}Cs source, in the presence or absence of 10 nM of the phosphatase inhibitor Calyculin A. For Western analyses, TATA binding protein (TBP) was used as a nuclear loading control.

The alterations observed in cell cycle control in *top3β*$^{-/-}$ cells led us to evaluate signaling pathways important for response to DNA damage. We assessed ataxia-telangiectasia, mutated (ATM)-dependent and ATM and Rad3-related (ATR)-dependent phosphorylation by using an fluorescent antibody recognizing phosphorylated substrates of ATM and ATR, and we observed a substantial, statistically significant decrease in nuclear foci in *top3β*$^{-/-}$ compared with *TOP3β*$^{+/+}$ control cells after either ionizing or UV-B radiation (Fig. 4). We then measured the induction of both total and Ser-18 [the murine analog to human Ser-15 (28)] phosphorylated p53 after the induction of DNA damage with either ionizing radiation or UV-B radiation. As expected, in *TOP3β*$^{+/+}$ control cells both total and phosphorylated p53 are induced after both agents, consistent with a crucial role for p53 in facilitating the G_1/S checkpoint. Surprisingly, total and Ser-18-phosphorylated p53 induction was defective in *top3β*$^{-/-}$ cells after ionizing radiation treatment (Fig. 5*A*), and a particularly marked defect was observed after UV-B irradiation (Fig. 5*B*). In addition, the induction of p21, a downstream target of p53, after ionizing or UV-B radiation in *top3β*$^{-/-}$ MEFs was substantially diminished compared with *TOP3β*$^{+/+}$ control MEFs, reflecting the defective activation of p53 in the context of DNA damage (Fig. 5).

Although the decreased proliferation rate of *top3β*$^{-/-}$ MEFs (≈2-fold relative to *TOP3β*$^{+/+}$ control MEFs) could contribute to this decreased p53 activation, the extent of this defect in p53 engagement is more extensive than that expected from proliferation rate alone and remains after normalizing to β-actin. Thus, in addition to its role in repair after DNA damage, we now provide evidence for a role of Top3β in the activation of the cellular response to DNA damage.

Discussion

The functions of DNA topoisomerases are a direct consequence of the requirement for DNA strands to unwind in the context of virtually all transactions involving DNA, including transcription, replication, and recombination. Notably, the type IA topoisomerases have been implicated in the regulation of genomic stability in lower eukaryotes, but the function of the two mammalian homologs of yeast Top3, Top3α and Top3β, remain incompletely understood.

The type IA topoisomerases mediate the sequential breakage and rejoining of individual DNA strands and are ideally suited for the resolution of DNA recombination intermediates such as double-Holliday junctions and other structures resulting from the repair of DNA double-strand breaks in the context of homologous recombination. Our studies of *top3β*$^{-/-}$ cells indicate that Top3β functions in the repair of DNA double-strand breaks, as evidenced by increased sensitivity of *top3β*$^{-/-}$ MEFs to ionizing radiation and increased baseline and postionizing radiation levels of phosphorylated γ-H2AX compared with *TOP3β*$^{+/+}$ control MEFs (Figs. 1*B* and 2). Type IA topoisomerases have also been implicated in the resolution of stalled or collapsed replication forks resulting from damage incurred in S phase (1, 29), and the increased sensitivity of *top3β*$^{-/-}$ versus *TOP3β*$^{+/+}$ control cells to UV-B radiation and hydroxyurea is consistent with this hypothesis (Fig. 1 *C* and *D*).

Notably, we also observed that enforcement of the G_1/S cell cycle checkpoint was incomplete in *top3β*$^{-/-}$ cells (Fig. 3), with inappropriate entry of *top3β*$^{-/-}$ cells into S phase 16 h after ionizing radiation treatment. However, the G_2/M and intra-S-phase check-

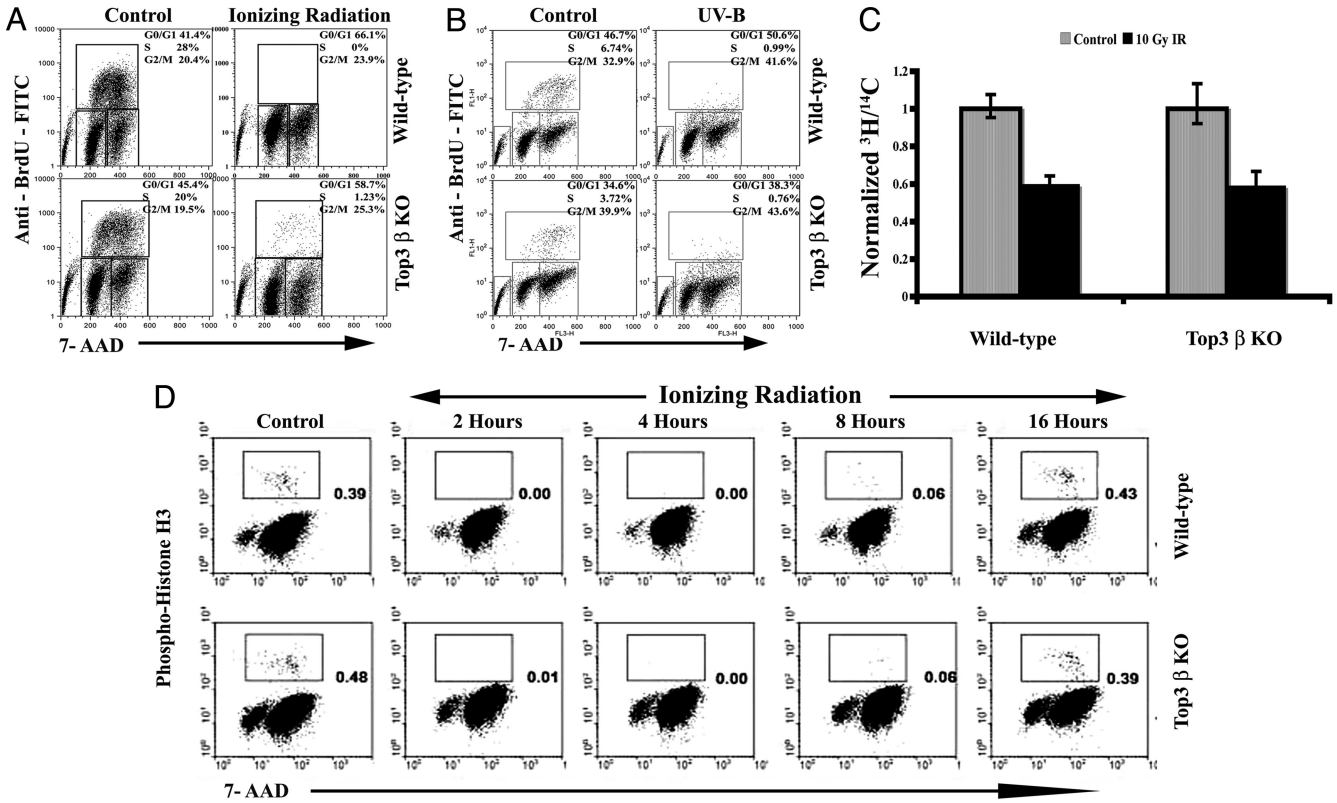

Fig. 3. Analysis of cell cycle checkpoints in *top3β*$^{-/-}$ cells. (*A*) Incomplete enforcement of the G_1/S cell cycle checkpoint in *top3β*$^{-/-}$ cells. Shown are flow cytometry plots of *TOP3β*$^{+/+}$ control (WT, *Upper*) and *top3β*$^{-/-}$ (*Lower*) MEFs pulsed with BrdU 18 h after 10 Gy of ionizing radiation. (*B* and *C*) Intact S-phase cell cycle checkpoint in *top3β*$^{-/-}$ cells. (*B*) Flow cytometry plots of *TOP3β*$^{+/+}$ control (WT, *Upper*) and *top3β*$^{-/-}$ (*Lower*) MEFs pulsed with BrdU 2 h after irradiation with 350 J/m^2 of UV-B are shown. (*C*) Assessment of radio-resistant DNA synthesis, as measured in *TOP3β*$^{+/+}$ control (WT, *Left*) and *top3β*$^{-/-}$ (*Right*) MEFs labeled with methyl-^{14}C-thymidine for 24 h, treated with 10 Gy ionizing radiation, then pulsed with methyl-^{3}H-thymidine for 30 min 1 h after irradiation. Normalized ^{3}H/^{14}C cpm ratios relative to untreated cells are depicted, with error bars indicating standard error of the mean. (*D*) Intact G_2/M cell cycle checkpoint in *top3β*$^{-/-}$ cells. *TOP3β*$^{+/+}$ control (WT, *Upper*) and *top3β*$^{-/-}$ (*Lower*) MEFs were irradiated with 5 Gy of ionizing radiation and at the indicated time points after irradiation were stained with anti-phospho-histone H3 antibody and 7-AAD for flow cytometry.

point responses appeared grossly unperturbed. In *S. cerevisiae*, an inappropriate acceleration in S-phase progression was observed in top3 cells after the induction of DNA damage, also suggesting a role for Top3 in the enforcement of cell cycle checkpoints (4, 30). The effect of Top3β deficiency on enforcement of the G_1–S checkpoint may reflect differential roles for Top3α and Top3β and the activity of p53 in mammalian cells. In this context, the fundamental role of p53 in mediating the G_1/S checkpoint in mammalian cells led us to evaluate p53 engagement after the induction of DNA damage in *top3β*$^{-/-}$ MEFs (31). Because *top3β*$^{-/-}$ cells have increased levels of DNA damage as manifested by phosphorylation of γ-H2AX, we expected to find intact or increased p53 engagement in such cells; instead, we observed that the up-regulation of both total and Ser-18 phosphorylated p53 was defective in *top3β*$^{-/-}$ cells treated with both ionizing and, particularly, UV-B radiation (Fig. 5). Moreover, we observed markedly decreased ATM/ATR-dependent phosphorylation after the induction of DNA damage in *top3β*$^{-/-}$ cells, although the recruitment of H2AX to sites of DNA double-strand breaks appeared intact and indeed enhanced in such cells (Figs. 2 and 4). Taken together, these results suggest that Top3β plays an unanticipated role in facilitating the transduction of signals resulting from DNA damage to the p53 effector response.

Decreased p53 activation in this setting could result from several potentially interrelated mechanisms. Because Ser-15/18 phosphorylation of p53 is ATM- and ATR-dependent (32–34), it is attractive to speculate that the decreased phosphorylation we have observed is a consequence of decreased ATM and ATR kinase activity. However, it is also possible that Top3β-mediated repair of a DNA damage intermediate may be required for optimal activation of ATM and ATR, and subsequent p53 engagement. Alternatively, the diminished immunofluorescence observed by using the ATM/ATR substrate antibody in *top3β*$^{-/-}$ cells after DNA damage could also suggest a potential function for Top3β in mediating the formation of nuclear foci indicative of ATM and ATR transduction complexes. In this context, the reduced number of positive nuclei in *top3β*$^{-/-}$ cells (see Fig. 4) likely is an underestimate of ATM/ATR substrate phosphorylation, because cells were scored as positive regardless of the intensity of fluorescence. Finally, a direct interaction between Top3β and p53 remains a possibility, although at present we have no evidence for such an association.

Although our results are consistent with a function for Top3β in DNA repair processes, they also suggest a previously unanticipated role for Top3β in the signal transduction response to DNA damage, and thereby provide evidence for a plausible link between Top3β and regulation of the G_1/S transition in the maintenance of genomic stability. Whether our findings reflect a combination of differential roles for Top3β and Top3α, the two mammalian type IA topoisomerases, and/or compensatory functions mediated by Top3α in the absence of Top3β activity remains to be determined in future studies.

Materials and Methods

Mice. Mice lacking Top3β were maintained in a specific pathogen-free environment at the Yale Animal Resource Center, Yale University School of Medicine. These mice were originally generated in a 129 × C57BL/6 back-

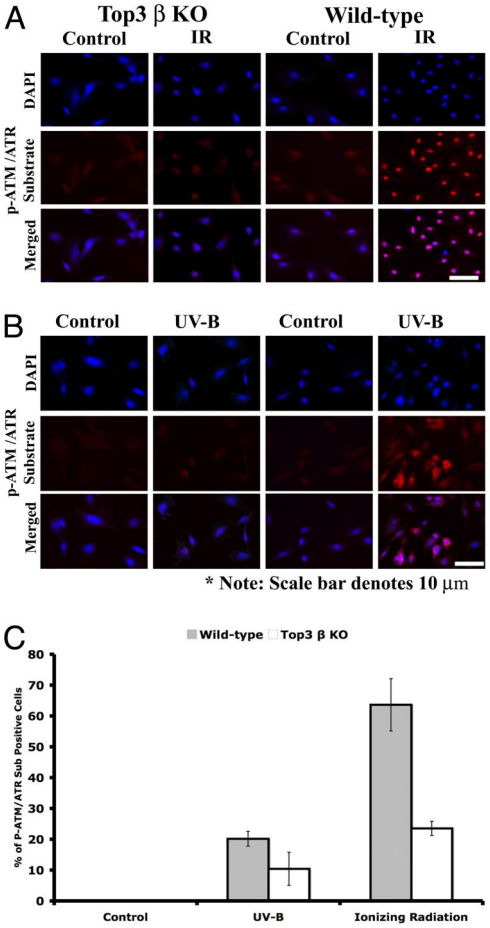

Fig. 4. Decreased ATM/ATR-dependent phosphorylation in *top3β*$^{-/-}$ cells. (*A* and *B*) Immunofluorescence microscopy analyses of *TOP3β*$^{+/+}$ control (WT, *Right*) and *top3β*$^{-/-}$ (*Left*) MEFs for phosphorylated ATM/ATR substrates (pATM/ATR) 30 min after 10 Gy of ionizing radiation (*A*) and 30 min after 1,000 J/m^2 UV-B radiation (*B*). DAPI nuclear staining (blue signal), phospho-ATM/ATR substrate (red signal), and merged images are shown. In three independent experiments using MEFs derived from three independent pairs of WT and *top3β*$^{-/-}$ embryos, we observed a statistically significant decrease in pATM/ATR substrate-positive fluorescence after the induction of DNA damage. (*C*) After UV-B irradiation, 100 of 674 pATM/ATR substrate and DAPI double-positive *top3β*$^{-/-}$ nuclei (14.4%) were observed compared with 429/1754 *TOP3β*$^{+/+}$ control nuclei (24.4%, $P = 0.0013$); after ionizing radiation, 149/548 *top3β*$^{-/-}$ (27%) compared with 1120/2014 (55.6%, $P = 0.0003$) *TOP3β*$^{+/+}$ control double-positive nuclei were scored. DAPI-positive nuclei showing any pATM/ATR fluorescence were scored as positive.

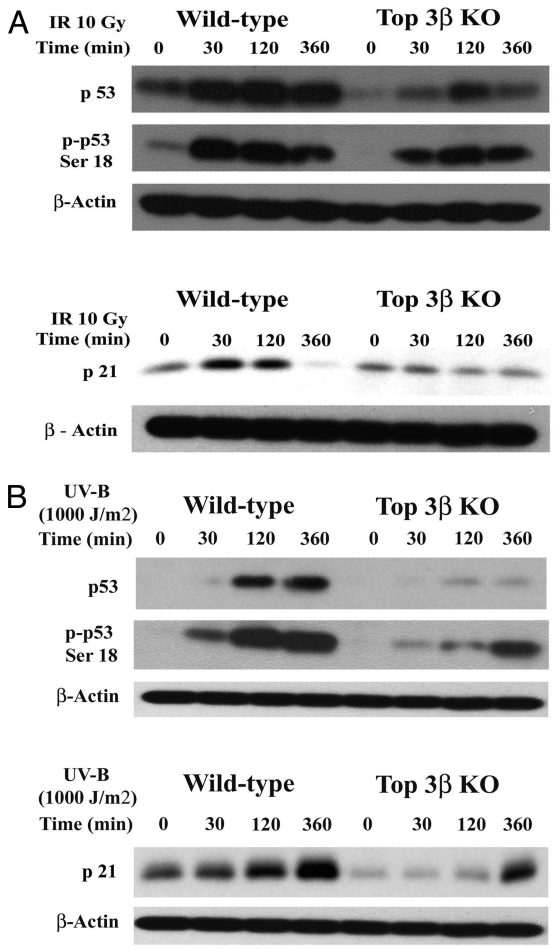

Fig. 5. Impaired p53 engagement in *top3β*$^{-/-}$ cells after the induction of DNA damage. Western blot analyses of *TOP3β*$^{+/+}$ control (WT) and *top3β*$^{-/-}$ MEFs after 10 Gy of ionizing radiation (*A*) or 1,000 of J/m^2 UV-B radiation (*B*) are shown. Both total and Ser-18-phosphorylated p53 are decreased in *top3β*$^{-/-}$ cells compared with *TOP3β*$^{+/+}$ control, and the induction of p21 is also defective after treatment with both DNA-damaging agents. β-Actin is shown as a loading control.

ground and had been backcrossed to C57BL/6 for five generations. Genotyping of mice was carried out via a PCR-based assay as described (26).

Culture of MEFs. Embryos were harvested on embryonic day 13.5 and placed separately in PBS. The fetal liver was removed by forceps to avoid contamination from hepatocytes and was used for genotyping of the embryos. The remaining portion of the embryo was minced, subsequently placed in a 15-ml conical tube carrying 0.25% trypsin EDTA (GIBCO), and incubated at 37°C for 1 h with intermittent pipetting to generate single-cell suspensions and allow debris to settle. The suspended cells were transferred to a fresh 50-ml tube containing 25 ml of DMEM (supplemented with 10% FBS, penicillin, streptomycin, 40 mM L-glutamine, 2 mM nonessential amino acids, 20 mM sodium pyruvate, 200 mM Hepes buffer, and 0.6% β-mercaptoethanol), washed twice with DMEM, and finally plated in a 10-cm culture dish. The next day, the medium was changed with pipetting to remove nonadherent cells. Cells at the second passage (P2) were grown to near confluence, harvested by trypsinization, and frozen in 10% DMSO in liquid nitrogen.

Such P2 MEFs were thawed and seeded as described for all analyses described below. For analysis of cell growth, *TOP3β*$^{+/+}$ control and *top3β*$^{-/-}$ MEFs (2×10^4 cells in DMEM) were seeded onto six-well plates in duplicate; on days 2, 4, 6, and 8, cells were harvested by trypsinization, and live cells were counted by using the trypan blue dye exclusion method.

Radiation Sensitivity Assay. Briefly, *TOP3β*$^{+/+}$ control and *top3β*$^{-/-}$ MEFs (2×10^5 cells in DMEM) were seeded onto 6-cm dishes in triplicate. The next day, MEFs were irradiated with differing dosages of ionizing radiation (ranging from 0 to 500 rads) by using a ^{137}Cs γ-ray source. After irradiation, medium in each plate was replaced with fresh warm medium, and cultures were incubated for 7 days at 37°C with a change in media at day 3. At the end of the assay period, MEFs were harvested by trypsinization, and viable cells were counted as described above.

Sensitivity to UV-B radiation was assessed as described, with some modifications (35). *TOP3β*$^{+/+}$ control and *top3β*$^{-/-}$ MEFs were seeded in triplicate onto six-well plates at 2×10^5 cells per well in DMEM and allowed to grow to ≈70% confluence. The medium was replaced with PBS, and MEFs were irradiated with varying dosages of UV-B (ranging from 0 to 1,000 J/m^2). After irradiation, the MEFs were supplied with fresh, warm DMEM and allowed to grow for 3 days. On day 3, viable MEFs were counted as discussed above.

For sensitivity to hydroxyurea (HU), *TOP3β*$^{+/+}$ control and *top3β*$^{-/-}$ MEFs were allowed to attach to plates at a density of 2×10^5 per well in six-well plates in triplicate. At ≈60–70% confluence, the medium was replaced with DMEM containing varying concentrations of HU (from 0 to 500 μM) for 24 h. After incubation with HU, MEFs were supplied with fresh DMEM without HU and allowed to grow for 2 more days, and the viable cells were counted as outlined above.

Analysis of p53 After Genotoxic Stress. MEFs were seeded in 6-cm dishes, grown to 80% confluence in DMEM, and subjected to either 10 Gy of ionizing radiation from a ^{137}Cs γ-ray source or 1,000 J/m^2 UV-B. At specific time points (30, 120, and 360 min) MEFs were harvested by trypsinization and washed twice with cold PBS. Cells were lysed in 20 mM Tris·HCl buffer (pH 8.0), 100 mM NaCl, 0.1% Triton X-100, 10 mM NaF, 1 mM Na_3VO_4, 1 mM PMSF, and 1× Complete protease inhibitors (Roche) on ice. After lysis, the samples were centrifuged at 9,279 × *g* at 4°C for 20 min. The cell extract was then boiled in SDS sample buffer for 5 min, fractionated by 10% SDS/PAGE, and transferred to PVDF membranes (Millipore). Membranes were blocked for 1 h at room temperature with 1× PBS containing 0.1% Tween-20 and 5% nonfat milk powder and incubated overnight at 4° C with slow rocking in 1×PBS, 0.1% Tween-20, and 5% BSA (Sigma) containing primary antibodies [anti-p53 mAb (clone IC12), rabbit anti-phospho-Ser-15-p53 Ab (both from Cell Signaling Technology) and monoclonal anti-p21 (clone SX118) from BD PharMingen]. After washing, the membranes were incubated with HRP-conjugated anti-mouse IgG (H+L) or anti-rabbit IgG (H+L) secondary antibodies (Zymed) for 1 h at room temperature, washed, and developed by using a chemiluminescent reagent (Amersham) followed by exposure to Kodak Biomax XAR film. For the β-actin control, membranes were stripped of the bound antibodies and probed with anti-mouse β-actin mAb (clone AC74; Sigma) for 1 h at in 1×TBS, 0.1% Tween-20, and 5% milk powder followed by an HRP-conjugated anti-mouse secondary antibody.

Cell Cycle Checkpoint Analyses. For assessment of the G_1/S checkpoint, MEFs at 70% confluence were incubated with medium containing 0.1% FBS for 72 h, then replated overnight in 6-cm dishes containing fresh growth medium supplemented with 10% FBS. MEFs were then either mock-treated or irradiated with 10 Gy from a ^{137}Cs γ-ray source. Eighteen hours after radiation, MEFs were pulsed with 10 μM BrdU for 1 h at 37°C and then harvested and processed for FACS analysis by using the FITC BrdU Flow Kit (BD Pharmingen) following the manufacturer's instructions. Acquisition of data was made with a BD FACS Calibur machine, and analysis used FlowJo software (Treestar).

For evaluation of the intra-S-phase checkpoint, MEFs were irradiated with 350 J/m^2 UV-B in PBS, pulsed with BrdU as described above 2 h postirradiation, and then processed for FACS analysis. Assessment of radio-resistant DNA synthesis was performed as described (36, 37) with slight modification. Briefly, 70% confluent MEFs were incubated with growth medium containing 0.0125 μCi methyl-^{14}C-thymidine (GE Healthcare) for 24 h, then harvested and replated in 6-cm dishes in equal number. After 24 h the MEFs were either mock-treated or irradiated with 10 Gy from an ^{137}Cs γ-ray source. One hour after IR treatment, MEFs were pulsed with 15 μCi of methyl-^{3}H-thymidine (GE Healthcare) for 30 min. Cells were then washed with medium/PBS and trypsinized in solutions containing 2.5 mM cold thymidine. Dual-labeled cells were processed in a cell harvester, and radioactivity was measured with a 1450 MicroBeta Tilux scintillation counter (PerkinElmer); the ^{3}H/^{14}C ratio was calculated after correction for channel cross-over as described (36).

For interrogation of the G_2/M checkpoint, MEFs at 60–70% confluence were treated with 5 Gy of ionizing radiation and at the timepoints indicated, they were fixed and permeabilized by using Cytofix/Cytoperm buffer (BD PharMingen). The cells were stained with Alexa Fluor 647 antiphosphorylated histone H3 (S-10) antibody and 7-aminoactinomycin D (7-AAD) and analyzed by flow cytometry.

Ionizing Radiation-Induced Phosphorylation of Histone H2AX. MEFS grown in the presence or absence of 10 nM Calyculin A (Sigma) were treated with 10 Gy of ionizing radiation from a ^{137}Cs γ-ray source; 30 min later, cells were harvested, fixed, permeabilized, and stained with FITC-conjugated anti-phospho Ser-139 histone H2-AX antibody (Upstate) and propidium iodide per the manufacturer's protocol for analysis by flow cytometry.

For Western analysis, cells were harvested, washed in PBS, and lysed in 20 mM Tris·HCl buffer (pH 8.0), 100 mM NaCl, 0.1% Triton X-100, 10 mM NaF, 1 mM Na_3VO_4, 1 mM PMSF, and 1× Complete protease inhibitors (Roche) on ice. After lysis, the samples were centrifuged at 9,279 × *g* at 4°C for 20 min. The pellet was washed with cold lysis buffer, resuspended in 0.2 M HCl, and incubated overnight at 4°C. Western analysis of acid-extracted proteins was carried out by using a rabbit anti-phospho-Ser-139 H2-AX antibody (Cell Signaling Technology), with a mAb against TBP (clone 17; BD Biosciences) used as a control.

Immunofluorescence Microscopy. Immunofluorescence microscopic analysis of irradiated and nonirradiated *TOP3*$\beta^{+/+}$ control and *top3*$\beta^{-/-}$ MEFs was carried out as described (38) with a polyclonal rabbit anti-phospho-(Ser/Thr) ATM/ATR substrate antibody (Cell Signaling Technology). MEFs were plated onto glass coverslips for attachment before irradiation. After irradiation with either ionizing radiation or UV-B, cells were fixed with 3% paraformaldehyde at room temperature for 20 min, washed with DMEM containing 10 mM Hepes (pH 7.4) three times for 5 min each, and then incubated with permeabilization buffer [DMEM containing 10% FBS, 10 mM Hepes (pH 7.4), 10 mM glycine, and 0.05% saponin (Sigma)] for 15 min at room temperature. The fixed and permeabilized cells were incubated with the ATM/ATR-phosphorylated substrate antibody (diluted in permeabilization buffer) overnight at 4° C, washed three times for 5 min each with permeabilization buffer, and incubated with Alexa Fluor 546-conjugated anti-rabbit IgG (Invitrogen) for 1 h at room temperature. Cells were washed three times with permeabilization buffer and mounted with VectaShield (Vector Laboratories) containing DAPI. Images were acquired under dark field with an automated Olympus BX-61 microscope, and analysis was carried out with Adobe Photoshop CS2 software.

For statistical analyses comparing pATM/ATR phosphorylation in *TOP3*$\beta^{+/+}$ control and *top3*$\beta^{-/-}$ MEFs after either ionizing or UV-B radiation, we used an exact Wilcoxon nonparametric test. The proportion of pATM/ATR substrate-positive fluorescence to the total number of DAPI-positive cells in three microscopic fields was assessed in three independent experiments with independently derived WT and *top3*$\beta^{-/-}$ MEFs. All statistical tests were two-tailed, and $P < 0.05$ was considered to indicate statistical significance. All analyses were performed with SAS version 9.1 (SAS Institute).

ACKNOWLEDGMENTS. We thank Dr. James C. Wang (Harvard University) for providing Top3β-deficient mice and helpful comments on the manuscript. This work was supported by National Institutes of Health Grant RO1 AG025142 (to A.C.S.). T.T. is supported by National Institutes of Health/National Institute on Aging''Pathway to Independence'' Award 1 K99 AG029726-01. R.A.F. is an Investigator of the Howard Hughes Medical Institute.

1. Wang JC (2002) Cellular roles of DNA topoisomerases: A molecular perspective. *Nat Rev Mol Cell Biol* 3:430–440.
2. Champoux JJ (2001) DNA topoisomerases: Structure, function, and mechanism. *Annu Rev Biochem* 70:369–413.
3. Champoux JJ (2002) Type IA DNA topoisomerases: Strictly one step at a time. *Proc Natl Acad Sci USA* 99:11998–12000.
4. Chakraverty RK, *et al.* (2001) Topoisomerase III acts upstream of Rad53p in the S-phase DNA damage checkpoint. *Mol Cell Biol* 21:7150–7162.
5. Gangloff S, de Massy B, Arthur L, Rothstein R, Fabre F (1999) The essential role of yeast topoisomerase III in meiosis depends on recombination. *EMBO J* 18:1701–1711.
6. Gangloff S, McDonald JP, Bendixen C, Arthur L, Rothstein R (1994) The yeast type I topoisomerase Top3 interacts with Sgs1, a DNA helicase homolog: A potential eukaryotic reverse gyrase. *Mol Cell Biol* 14:8391–8398.
7. Wallis JW, Chrebet G, Brodsky G, Rolfe M, Rothstein R (1989) A hyper-recombination mutation in *S. cerevisiae* identifies a novel eukaryotic topoisomerase. *Cell* 58:409–419.
8. Goodwin A, Wang SW, Toda T, Norbury C, Hickson ID (1999) Topoisomerase III is essential for accurate nuclear division in *Schizosaccharomyces pombe*. *Nucleic Acids Res* 27:4050–4058.
9. Maftahi M, *et al.* (1999) The top3(+) gene is essential in *Schizosaccharomyces pombe* and the lethality associated with its loss is caused by Rad12 helicase activity. *Nucleic Acids Res* 27:4715–4724.
10. Oh M, Choi IS, Park SD (2002) Topoisomerase III is required for accurate DNA replication and chromosome segregation in *Schizosaccharomyces pombe*. *Nucleic Acids Res* 30:4022–4031.
11. Win TZ, Goodwin A, Hickson ID, Norbury CJ, Wang SW (2004) Requirement for *Schizosaccharomyces pombe* Top3 in the maintenance of chromosome integrity. *J Cell Sci* 117:4769–4778.
12. Bennett RJ, Noirot-Gros MF, Wang JC (2000) Interaction between yeast sgs1 helicase and DNA topoisomerase III. *J Biol Chem* 275:26898–26905.
13. Fricke WM, Kaliraman V, Brill SJ (2001) Mapping the DNA topoisomerase III binding domain of the Sgs1 DNA helicase. *J Biol Chem* 276:8848–8855.
14. Watt PM, Hickson ID, Borts RH, Louis EJ (1996) SGS1, a homologue of the Bloom's and Werner's syndrome genes, is required for maintenance of genome stability in *Saccharomyces cerevisiae*. *Genetics* 144:935–945.
15. Shor E, *et al.* (2002) Mutations in homologous recombination genes rescue top3 slow growth in *Saccharomyces cerevisiae*. *Genetics* 162:647–662.
16. Zhu Q, Pongpech P, DiGate RJ (2001) Type I topoisomerase activity is required for proper chromosomal segregation in *Escherichia coli*. *Proc Natl Acad Sci USA* 98:9766–9771.
17. Harmon FG, DiGate RJ, Kowalczykowski SC (1999) RecQ helicase and topoisomerase III comprise a novel DNA strand passage function: A conserved mechanism for control of DNA recombination. *Mol Cell* 3:611–620.
18. Ira G, Malkova A, Liberi G, Foiani M, Haber JE (2003) Srs2 and Sgs1-Top3 suppress cross-overs during double-strand break repair in yeast. *Cell* 115:401–411.
19. Johnson FB, *et al.* (2000) Association of the Bloom syndrome protein with topoisomerase IIIα in somatic and meiotic cells. *Cancer Res* 60:1162–1167.
20. Wu L, *et al.* (2006) BLAP75/RMI1 promotes the BLM-dependent dissolution of homologous recombination intermediates. *Proc Natl Acad Sci USA* 103:4068–4073.
21. Wu L, *et al.* (2000) The Bloom's syndrome gene product interacts with topoisomerase III. *J Biol Chem* 275:9636–9644.

22. Wu L, Hickson ID (2002) The Bloom's syndrome helicase stimulates the activity of human topoisomerase IIIα. *Nucleic Acids Res* 30:4823–4829.
23. Wu L, Hickson ID (2003) The Bloom's syndrome helicase suppresses crossing over during homologous recombination. *Nature* 426:870–874.
24. Kwan KY, *et al.* (2007) Development of autoimmunity in mice lacking DNA topoisomerase 3β. *Proc Natl Acad Sci USA* 104:9242–9247.
25. Kwan KY, Moens PB, Wang JC (2003) Infertility and aneuploidy in mice lacking a type IA DNA topoisomerase IIIβ. *Proc Natl Acad Sci USA* 100:2526–2531.
26. Kwan KY, Wang JC (2001) Mice lacking DNA topoisomerase IIIβ develop to maturity but show a reduced mean lifespan. *Proc Natl Acad Sci USA* 98:5717–5721.
27. Li W, Wang JC (1998) Mammalian DNA topoisomerase IIIα is essential in early embryogenesis. *Proc Natl Acad Sci USA* 95:1010–1013.
28. Chao C, Saito S, Anderson CW, Appella E, Xu Y (2000) Phosphorylation of murine p53 at Ser-18 regulates the p53 responses to DNA damage. *Proc Natl Acad Sci USA* 97:11936–11941.
29. Wu L, Hickson ID (2006) DNA helicases required for homologous recombination and repair of damaged replication forks. *Annu Rev Genet* 40:279–306.
30. Mankouri HW, Hickson ID (2006) Top3 processes recombination intermediates and modulates checkpoint activity after DNA damage. *Mol Biol Cell* 17:4473–4483.
31. Appella E, Anderson CW (2001) Posttranslational modifications and activation of p53 by genotoxic stresses. *Eur J Biochem* 268:2764–2772.
32. Banin S, *et al.* (1998) Enhanced phosphorylation of p53 by ATM in response to DNA damage. *Science* 281:1674–1677.
33. Canman CE, *et al.* (1998) Activation of the ATM kinase by ionizing radiation and phosphorylation of p53. *Science* 281:1677–1679.
34. Tibbetts RS, *et al.* (1999) A role for ATR in the DNA damage-induced phosphorylation of p53. *Genes Dev* 13:152–157.
35. Tian M, Jones DA, Smith M, Shinkura R, Alt FW (2004) Deficiency in the nuclease activity of xeroderma pigmentosum G in mice leads to hypersensitivity to UV irradiation. *Mol Cell Biol* 24:2237–2242.
36. Theunissen JW, Petrini JH (2006) Methods for studying the cellular response to DNA damage: Influence of the Mre11 complex on chromosome metabolism. *Methods Enzymol* 409:251–284.
37. Weiss RS, Leder P, Vaziri C (2003) Critical role for mouse Hus1 in an S-phase DNA damage cell cycle checkpoint. *Mol Cell Biol* 23:791–803.
38. DiTullio RA, Jr, *et al.* (2002) 53BP1 functions in an ATM-dependent checkpoint pathway that is constitutively activated in human cancer. *Nat Cell Biol* 4:998–1002.